A ^{31}P Dynamic NMR Study of the Bond Shift Rearrangement in Solid Li_3P_7

Tapas Sen,[†] Raphy Poupko,[†] Ulrich Fleischer,[‡] Herbert Zimmermann,[§] and Zeev Luz*,[†]

Contribution from the The Weizmann Institute of Science, Rehovot 76100, Israel, Department of Chemistry, University of Arkansas, Fayetteville, Arkansas 72701, and Max-Planck-Institut für Medizinische Forschung, AG Molekülkristalle, 69028 Heidelberg, Germany

Received July 12, 1999. Revised Manuscript Received October 19, 1999

Abstract: Phosphorus-31 NMR measurements are reported on solid $Li_3P_7(monoglyme)_3$ in the temperature range −90 to +70 °C, under both, nonspinning and magic angle spinning (MAS) conditions. At low temperatures (<−30 °C) the spectra correspond to a static situation, exhibiting a superposition of three subspectra due to the apical, equatorial, and basal phosphorus atoms in the P_7-cage. Analysis of these spectra provided information on the principal values of the chemical shift tensors of the various P atoms in their respective principal axis systems. Their orientations in the molecular frame were obtained from quantum mechanical calculations. In the temperature range −30 to +70 °C the spectra exhibit dynamic effects, which at high temperatures result in a line shape corresponding to a single average axially symmetric chemical shift tensor. This is interpreted in terms of a bond shift rearrangement similar to the Cope rearrangement process in bullvalene. Analysis of the results yields approximate kinetic parameters for the reaction. At room-temperature the rate constant is about 10^5 s^{-1}, and the activation energy lies between 7 and 12 kcal/mol. Due to the amorphous nature of the sample used and the incomplete fit of the experimental and simulated spectra, the possibility of a heterogeneous reaction with a distribution of rates and an independent 3-fold jumps process, cannot be ruled out.

Introduction

Several derivatives of the R_3P_7 family of compounds are known, including $(Me_3Si)_3P_7$, H_3P_7 and Li_3P_7.[1] In these compounds the P_7 moiety forms a cage-like structure (see Figure 1) with the R groups linked to the equatorial P-atoms. Li_3P_7 is known to exist in a number of solid modifications, one of which is a solvent-free, highly coordinated, substance with an ionic structure.[2] However, it mostly appears in the form of solvates with three bidentate solvent molecules per Li_3P_7 unit. The solvates usually precipitate from solution as amorphous solids. An exception is $Li_3P_7(tmeda)_3$ (tmeda = tetramethylethylenediamine) which was obtained in a crystalline form and could thus be studied by X-ray crystallography.[2] Its molecular structure is shown schematically in Figure 1a. The P_7-cage has C_{3v} symmetry, and the three Li^+ ions are each coordinated to two negatively charged equatorial P-atoms. The lithium ions occupy sites with pseudotetrahedral symmetry where two other bonds are shared with the bidentate ligand (solvent) molecule. Other compounds having related structures are the P_7 dimers, Sr_3P_{14} and Ba_3P_{14}.[3,4]

Baudler and co-workers,[5−7] using ^{31}P NMR have extensively studied the structure and dynamics of Li_3P_7 in solution. At low temperatures (<−30 °C) the spectrum consists of three spin−spin multiplets with relative intensities 1:3:3, centered around −57, −103, and −162 ppm (relative to 85% H_3PO_4). They correspond to, respectively, the apical (A), equatorial (E), and basal (B) phosphorus atoms (Figure 1b). The fine structure observed in the spectrum was quantitatively interpreted in terms of all possible $^1J_{PP}$'s and $^2J_{PP}$'s in the P_7-cage.[7] Some extra line broadening of the equatorial phosphorus signals was shown (by ^{6}Li isotopic substitution) to results from interactions with the ^{7}Li nuclei, which are partially self-decoupled by the quadrupolar relaxation of the latter.

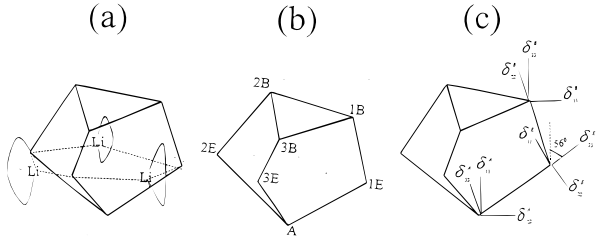

Figure 1. Structural formulas of the P_7-cage. (a) Schematic representation of the Li-bidentate solvate structures as determined by X-ray crystallography for the tmeda complex. (b) Labeling convention used for the P atoms in the P_7-cage. (c) PAS's for the apical (A), equatorial (E), and basal (B) P atoms in wing 1 (consisting of the A, 1E, and 1B atoms) of the P_7-cage.

Above −30 °C, the spectrum gradually broadens and eventually (at above 50 °C) it coalesces into a single narrow line at the weighted average frequency of the separate bands. This observation was interpreted[5] in terms of a bond shift rearrangement within the P_7-cage, similar to the well-known Cope rearrangement in bullvalene (see Figure 2).[8] The highly degenerate rearrangement reaction leads to complete averaging of the chemical shifts of all atoms in the P_7-cage and hence to a single NMR line. The reaction mechanism was subsequently

[†] The Weizmann Institute of Science.
[‡] University of Arkansas.
[§] Max-Planck-Institut für Medizinische Forschung.

(1) (a) Baudler, M. *Angew. Chem., Int. Ed. Engl.* **1982**, *21*, 492. (b) Baudler, M.; Glinka, K. *Chem. Rev.* **1993**, *93*, 1623.
(2) Honle, W.; Schnering, H. G. v.; Schmidpeter, A.; Burget, G. *Angew. Chem., Int. Ed. Engl.* **1984**, *23*, 817.
(3) Dahlmann, W.; Schnering, H. G. v. *Naturwissenschaften* **1972**, *59*, 420.
(4) Dahlmann, W.; Schnering, H. G. v. *Naturwissenschaften* **1973**, *60*, 429.
(5) Baudler, M.; Ternberger, W. F.; Hahn, J. *Z. Naturforsch.* **1979**, *34b*, 1690.
(6) Baudler, M.; Hahn, J. *Z. Naturforsch.* **1990**, *45b*, 1279.
(7) Baudler, M.; Pontzen, T.; Hahn, J.; Ternberger, W. F.; Faber, W. *Z. Naturforsch.* **1980**, *35b*, 517.

10.1021/ja992452l CCC: $19.00 © 2000 American Chemical Society
Published on Web 01/21/2000

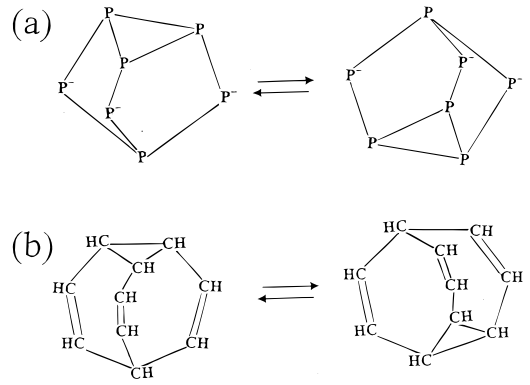

Figure 2. The bond shift (Cope) rearrangement in P_7 (a) and bullvalene (b).

also confirmed by 2D-exchange NMR.[6] This reaction was the first demonstration of a Cope-like rearrangement in an inorganic compound and so far is apparently also the only one. No full line shape analysis of the dynamic spectra in solution has been presented. However, the activation energy of the reaction was estimated[5] to lie between 10 and 15 kcal/mol and from the published spectra, the rate at room temperature can be estimated to be $\sim 10^4$ s^{-1}.

For bullvalene and many of its monosubstituted derivatives it was found, somewhat unexpectedly, that the Cope rearrangement also takes place in the solid state and that it proceeds in a way that preserves the crystal order.[9−15] This is brought about by a concomitant reorientation of the molecule which ensures that it ends up in the proper orientation in the crystal lattice.

In the present work we address the question of whether the bond shift rearrangement process, which was detected in solutions of Li_3P_7, also takes place in the solid state. It is believed that in solution the rearrangement involves free (unbound) P_7 anions.[2] In solid Li_3P_7 the P_7-cages are coordinated to Li ions, and it may appear that in this form the rearrangement reaction might be hindered. Here we show that this is definitely not the case and that, in fact, the reaction in the solid phase is even faster than it is in solution. For our measurements we use the solvate Li_3P_7(monoglyme)$_3$ (monoglyme = $CH_3OCH_2CH_2OCH_3$), which is commercially available in a noncrystalline, amorphous solid form. The ^{31}P NMR spectra of this solid showed conspicuous dynamic effects that indicated unequivocally the occurrence of bond shift rearrangement in the P_7-cage.

Experimental Section

Li_3P_7(monoglyme)$_3$ was obtained commercially from ACROS ORGANICS and used without further treatment. Samples for NMR measurements were prepared by packing the material into suitable containers in a glovebox saturated with nitrogen gas. For MAS experiments 4 mm spinners (containing ~65 mg material) were used with boron nitride caps. For the nonspinning NMR experiments 5 mm glass tubes were used, which were fire-sealed under vacuum while keeping the Li_3P_7 at liquid nitrogen temperature. Experiments were carried out up to +70 °C. Above this temperature the sample disintegrated, as manifested by its blackening and the fact that the NMR spectra became irreproducible.

The NMR measurements were performed on a Bruker DSX300 Spectrometer operating at a ^{31}P frequency of 121.5 MHz. Some ^{7}Li measurements were also carried out on this instrument at a frequency of 116.6 MHz. Additional experimental details are given in the relevant figure captions.

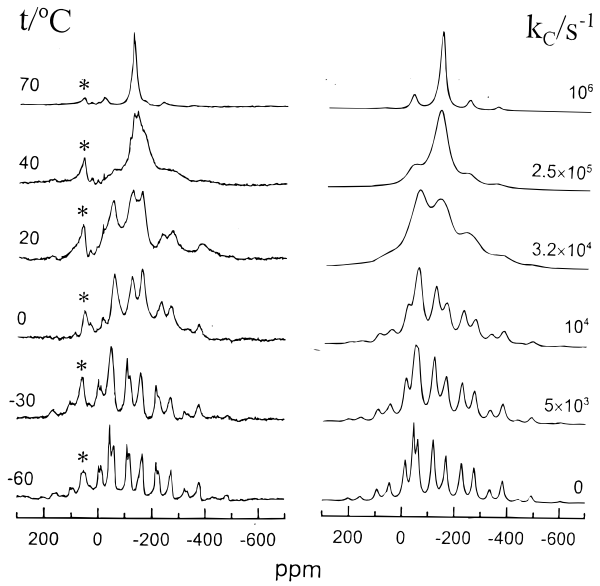

Figure 3. Left: Experimental ^{31}P MAS NMR spectra of Li_3P_7-(monoglyme)$_3$ as a function of the temperature, as indicated. Spinning frequency: 13.0 kHz. The spectra were obtained by single $\pi/2$ pulses (4 μs) with a recycle delay of 2 min. The number of scans ranged from 4, at low temperatures, to 16 at high temperatures. The asterisk indicates an impurity peak. The frequency scale in this and all others ^{31}P spectra is relative to 85% H_3PO_4. Right: Simulated dynamic MAS spectra for the indicated rate constants of the bond shift rearrangement. The simulations were done using the Floquet formalism with the chemical shift parameters given in Table 1. For each P atom, 13 Floquet states were used, requiring the diagonalization of a 91 × 91 matrix for each crystallite orientation. A total of 538 orientations were used. Different line width parameters were used for the three types of P-atoms, ranging from (full width at half-maximum height in Hz) 700 at low temperatures to 240 at high temperature for the apical atom, from 1000 to 300 for the equatorial and from 900 to 280 for the basal atoms.

Results and Discussion

The Low-Temperature Spectra and the Principal Values of the ^{31}P Chemical Shift Tensors. In Figures 3 and 4 are shown, respectively, ^{31}P NMR spectra of spinning (MAS) and nonspinning Li_3P_7(monoglyme)$_3$ samples as a function of the temperature. Both sets of spectra exhibit pronounced changes with temperature, which clearly reflect the onset of one or several dynamic processes. To analyze these effects we need first to understand the low-temperature spectra, where presumably the motion does not affect the spectral line shape.

The main terms in the ^{31}P spin Hamiltonian are those due to the (anisotropic) chemical shifts (CS), the dipolar interactions and the scalar couplings. In the P_7 moiety the latter are of the order of 400 Hz or less[7] and can be neglected in comparison with the line width in solid-state spectra. The dipolar interactions between neighboring P nuclei in the P_7 cage (with internuclear

(8) (a) Schröder, G.; Oth, J. F. M. *Angew. Chem.* **1967**, *458*, 79. (b) Oth, J. F. M.; Müllen, K.; Gilles, J. M.; Schröder, G. *Helv. Chim. Acta* **1974**, *57*, 1415. (c) Poupko, R.; Zimmermann, H.; Müller, K.; Luz, Z. *J. Am. Chem. Soc*. **1996**, *118*, 7995.

(9) Meier, B. H.; Earl, W. L. *J. Am. Chem. Soc.* **1985**, *107*, 5553.

(10) Schlick, S.; Luz, Z.; Poupko, R.; Zimmermann, H. *J. Am. Chem. Soc.* **1992**, *114*, 4315

(11) Titmann, J. J.; Luz, Z.; Spiess, H. W. *J. Am. Chem. Soc.* **1992**, *114*, 3765.

(12) Luz, Z.; Poupko, R.; Alexander, S. *J. Chem. Phys*. **1993**, *99*, 7544.

(13) Müller, A.; Haeberlen, U.; Zimmermann, H.; Poupko, R.; Luz, Z. *Mol. Phys*. **1994**, *81*, 1239.

(14) (a) Müller, K.; Zimmermann, H.; Krieger, C.; Poupko, R.; Luz, Z. *J. Am. Chem. Soc.* **1996**, *118*, 8006. (b) Poupko, R.; Müller, K.; Krieger, C.; Zimmermann, H.; Luz, Z. *J. Am. Chem. Soc.* **1996**, *118*, 8015. (c) Olivier, L.; Poupko, R.; Zimmermann, H.; Luz, Z. *J. Phys. Chem*. **1996**, *100*, 17995.

(15) Luz, Z.; Olivier, L.; Poupko, R.; Müller, K.; Krieger, C.; Zimmermann, H. *J. Am. Chem. Soc*. **1998**, *120*, 5526.

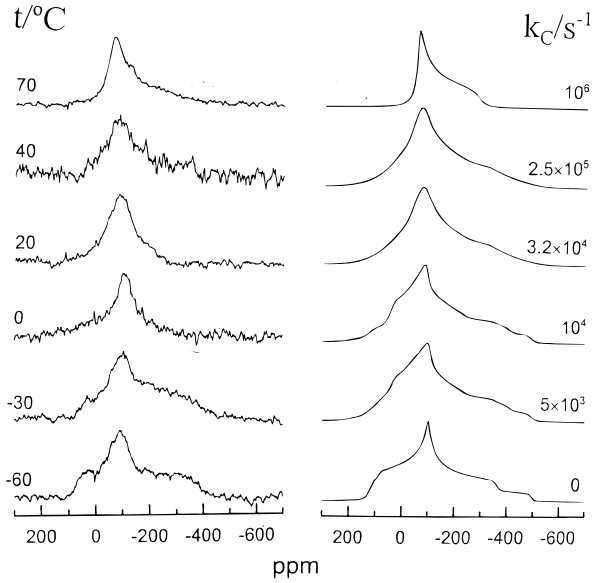

Figure 4. Left: Experimental ^{31}P NMR spectra of a nonspinning powder sample of $Li_3P_7(monoglyme)_3$ as a function of the temperature, as indicated. The spectra were recorded using short (2.1 μs) pulses followed by Fourier transformation. Recycle time, 2 min. The number of scans ranged from 60, at high and low temperatures, to 150, in the intermediate ranges. Right: Simulated dynamic powder spectra for different rate constants of the bond shift rearrangement, as indicated. The calculations were done using the magnetic parameters as described in the caption of Figure 3.

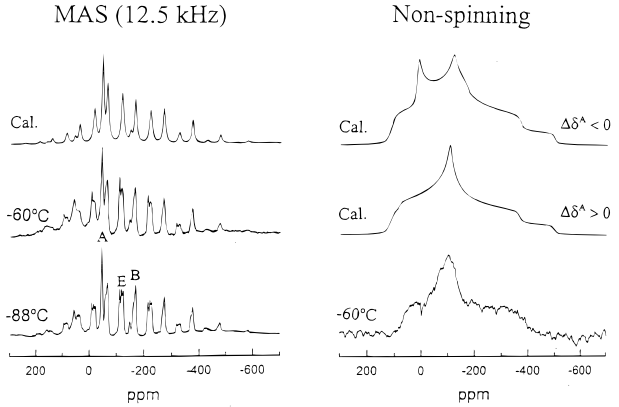

Figure 5. Left: ^{31}P MAS NMR spectra of $Li_3P_7(monoglyme)_3$ at a spinning frequency of 12.5 kHz. The bottom two spectra are experimental at very low temperature as indicated. The letters A, E and B mark the central peaks of the apical, equatorial and basal spinning sideband manifolds. Note the fine structure of the E-peaks due to interactions with the Li nuclei. The top trace is a simulated spectrum calculated using the chemical shift parameters of Table 1 and the low-temperature line width as indicated in the caption of Figure 3. Right: ^{31}P NMR spectra of a nonspinning sample of $Li_3P_7(monoglyme)_3$. The bottom spectrum is experimental for the indicated temperature. The two upper traces were simulated using the chemical shift parameters of Table 1A, but for two different signs of the chemical shift anisotropy of the apical P-atom, as indicated.

distances of about 2.15 Å) are of the order of 2 kHz. They are smaller for not directly bonded P atoms in the cage and considerably smaller for atoms in different molecules. Even though the multiple dipolar interactions within the P_7-cage may sum up to as much as 5 kHz, to a good approximation, they too may be neglected in comparison with the overall spectral width. This is particularly true in the MAS experiments, where the dipolar interactions are partially (although not completely[16]) averaged out by the spinning. On the other hand, the chemical shift anisotropy of the ^{31}P nuclei in P_7 are of the order of 20−75 kHz and are clearly the dominant terms in the phosphorus spin Hamiltonian. We therefore keep only the latter interactions in the quantitative analysis of the dynamic spectra.

To obtain the principal values of the chemical shift tensors of the various phosphorus atoms in the Li_3P_7 sample we analyzed the low-temperature MAS spectra, using the Herzfeld−Berger theory.[17] In Figure 5 are shown two such spectra recorded at −88 and −60 °C with a spinning frequency of 12.5 kHz. This spinning rate is close to the highest attainable value on our spectrometer. Under this restriction it provides the best resolution with minimum overlap of sidebands from different manifolds. The center bands of the three types of phosphorus atoms, apical (A), equatorial (B), and basal (C), are indicated on the bottom trace. From these the associated spinning sidebands can readily be identified.

Three points related to these spectra need be emphasized: (i) It may be noticed that the lines due to the equatorial atoms, which are closest to the lithium cations, exhibit an asymmetric multiplet; a triplet at −88 °C, which broadens into a doublet at −60 °C. We ascribe this structure to the residual dipolar (and scalar) interactions with the neighboring quadrupolar ^7Li nuclei, which are not averaged out by the magic angle spinning. Similar spectra have been observed before for ^{13}C coupled to $I = {}^3/_2$ nuclei.[18] We have not analyzed this structure quantitatively. Instead, we accounted for it by introducing an effective additional broadening to the lines associated with the equatorial atoms.

(ii) The second point to notice is the extra hump at around 64 ppm, which does not seem to belong to any of the three spinning sideband manifolds. It is particularly noticeable at higher temperatures where the P_7 peaks broaden while this one appears to gain in relative intensity (see Figure 3). We ascribe it to an unidentified impurity.

(iii) Finally, we notice that in the spectrum shown in Figure 5, only two very weak sidebands are observed for the apical atom, at −146 and +60 ppm (the latter closely overlapping with the impurity peak). This indicates that the CS anisotropy associated with this atom is considerably smaller than for the equatorial and the basal atoms. Also, because the apical atom sits on the molecular C_3 symmetry axis, its CS tensor should be axially symmetric. Since, however, its two spinning sidebands have nearly the same intensity, it is not possible to determine the sign of its CS anisotropy. This was subsequently determined from the line shape of the low-temperature spectrum of the nonspinning, sample (see below).

The overall results of the analysis are summarized in Table 1A, with $\delta_{11} > \delta_{22} > \delta_{33}$ (from less to more shielding). By and large, the CS tensors so obtained are of the order of those determined in similar compounds.[19−21] A simulated MAS spectrum calculated using these parameters is shown on the top left-hand side of Figure 5. Considering the points mentioned above the fit between the experimental and simulated spectra is quite satisfactory.

On the right-hand side of Figure 5 are shown the corresponding spectra for a nonspinning sample. At the bottom is shown an experimental spectrum recorded at −60 °C and two simulated

(16) Jeschke, G.; Hoffhauer, W.; Jansen, M. *Chem. Eur. J.* **1998**, *4*, 1755.
(17) Herzfeld, J.; Berger, A. E. *J. Chem. Phys.* **1980**, *73*, 6029.
(18) (a) Harris, R. K.; Olivieri, A. C. *Prog. Nucl. Magn. Reson. Spectrosc.* **1992**, *24*, 435. (b) Alarcon, S. H.; Olivieri, A. C.; Crass, S. A.; Harris, R. K.; Zuriaga, M. J.; Monti, G. A. *J. Magn. Reson.* **1995**, *116A*, 244.
(19) Spiess, H. W.; Grosescu, R.; Haeberlen, U. *Chem. Phys.* **1974**, *6*, 226.

Table 1. CS Tensors of the Various Phosphorus Atoms in Li_3P_7 [a]

1A. Principal Values in Their Respective PAS's

	basal				equatorial				apical			
	δ_{iso}	δ_{11}	δ_{22}	δ_{33}	δ_{iso}	δ_{11}	δ_{22}	δ_{33}	δ_{iso}	δ_{11}	δ_{22}	δ_{33}
exptl[b]	−167	276	56	−332	−119	244	2	−246	−43	126	−63	−63
calcd(1)[c]	−163	259	122	−380	−116	236	−26	−211	−7	18	−9	−9
calcd(2)[d]	−166	295	78	−373	−120	239	−52	−188	−35	58	−29	−29

1B. Euler Angles Which Transform the Various PAS's to the MF[e]

	basal			equatorial			apical		
	α	β	γ	α	β	γ	α	β	γ
simulated[f]	0	0	γ	0	−56	γ	0	0	0
calcd(1)[c]	0	2	γ	0	−52	γ	0	0	0
calcd(2)[d]	0	1	γ	0	−61	γ	0	0	0

[a] The subscripts 11, 22, 33, serve to label the principal values of the CS tensors according to the order $\delta_{11} > \delta_{22} > \delta_{33}$ (with $\delta_{11} + \delta_{22} + \delta_{33}=0$); they do not necessarily form a right-handed coordinate system. For their orientation in the MF see part 1B. [b] Experimental values derived from the MAS spectra of Li_3P_7(monoglyme)$_3$. [c] Calculated values for unsolvated Li_3P_7. [d] Calculated values for the solvate Li_3P_7(glycol)$_3$. [e] α, β, γ are Euler angles which transform the CS tensors from their respective PAS's, a^i, b^i, c^i, to the MF *x*, *y*, *z*. In this frame, *z* is parallel to the C_3 symmetry axis, *y* is perpendicular to the plane of wing 1, defined by the atoms, 1B, 1E, A, and *x* lies in the plane of this wing. The PAS axes for the B and E atoms were chosen so that a^i lies in the plane of the *i*th wing, b^i perpendicular to this wing, and c^i perpendicular to both axes. For the apical atom, *a*, *b*, and *c* coincide with the *x*, *y*, *z*, system. The sets, a^i, b^i, c^i, as well as *x*, *y*, *z* form right-handed coordinate systems. γ equals 0°, 240°, and 120° for the B and E atoms in wings 1, 2, and 3, respectively. [f] Values used in the line shape simulations.

traces shown above it. They were calculated using the (experimental) CS parameters from Table 1A, but for two alternative signs for the anisotropy of the apical atom, −126, 63, 63 (top) and 126, −63, −63 (middle). As mentioned above this sign could not be determined from the MAS spectrum at low temperatures. Comparison of the simulated powder spectra with the experimental one confirms unequivocally the sign chosen in Table 1. The general agreement of the experimental and simulated powder line shapes is, however, not as satisfactory as for the MAS spectra. In particular the high-field shoulders (at −360 and −500 ppm) and the center cusp (at −100 ppm) in the simulated trace are not as pronounced in the experimental spectrum. Also, the low-field edge is somewhat shifted to the right in the simulation compared to the experiment. The former effects are most likely due to the neglect of P−P dipolar and scalar interactions. When these interactions were included in the simulation the fit of the high-field part of the spectrum considerably improved, but the shift in the low-field edge remained. We ascribe this disagreement to the uncertainty (∼10 ppm) in the experimentally determined principal values of the basal and equatorial CS tensors (Table 1A). The uncertainty for the apical atom is probably larger, but it affects less the overall width of the spectrum.

The Orientation of the Principal Components of the CS Tensors. The results of the previous section provide the values of the CS tensor components in their respective principal axis system (PAS). For a complete analysis of the dynamic line shapes we also need to know the orientations of the PAS's in a common molecular frame (MF). In principle this can be obtained by measurements of single crystals, but these have not been available to us. Instead, we resorted to quantum mechanical calculations. The idea being that for the simulation of the dynamic spectra we shall use the principal values as determined by the experiments, but adopt the directions provided by the theory.

For the calculations we used the IGLO method.[22,23] They were carried out at the Hartree−Fock level using a basis set of roughly triple-ζ quality, supplemented with polarization functions.[23] Several model compounds were studied, but we shall report on just two: (1) free (nonsolvated) Li_3P_7 and, to check on the effect of the ligands, (2) Li_3P_7 coordinated to three glycol (1,2-dihydroxyethane) molecules. The structure of the model compounds was first optimized at the DFT level, with a 6-31G* basis set (using B3LYP as implemented in the GAUSSIAN 94 package of programs).[22,23] A constraint to C_{3v} symmetry was applied throughout the optimizations, with the Li and ligand molecules as in structure (a) of Figure 1. The structural parameters so obtained are in good agreement with those determined experimentally for Li_3P_7(tmeda)$_3$ by X-ray crystallography.[2] The P−P distances in the former are about 0.05 Å larger than in the latter. Similar results were also obtained by Böhm and Gleiter,[24] who used the semiempirical MINDO/3 program to calculate the P_7 structure.

The results of the calculations of the CS tensors for the two model compounds are included in Table 1. The principal values for the various atoms, in their respective PAS's, are given in part 1A of the Table, while the Euler angle relating the PAS's with the MF are given in 1B. In general the agreement between the experimental principal values and those calculated for both models, although far from perfect, is quite sufficient for our purpose. In particular, the differences between the principal values for each atom are large enough to allow unequivocal matching of the experimental components with the corresponding calculated ones, as given in Table 1A. The differences between the two sets of calculations, for the basal and equatorial atoms, are of the same order as their deviation from the experimental values. Although in some cases, these deviations are as large as 60 ppm, they are small compared to the overall CS anisotropy. On the other hand, the results for the Euler angles of the two models (Table 1B) are quite similar, deviating by only a few degrees from each other. For that reason (and also for lack of alternative methods to determine them) we adopt

(20) (a) Gibby, M. G.; Pines, A.; Rhim, W.-K.; Waugh, J. S. *J. Chem. Phys*. **1972**, *56*, 991. (b) Zumbulyadis, N.; Dailey, B. P. *Chem. Phys. Lett*. **1974**, *26*, 273. (c) Eckert, H.; Liang, C. S.; Stuky, G. D. *J. Phys. Chem.* **1989**, *93*, 452. (d) Harris, R. K.; Wilkes, P. J.; Wood, P. T.; Woollins, J. D.; *J. Chem. Soc., Dalton Trans.* **1989b**, 809. (e) Bjorholm, T.; Jakobsen, H. J. *J. Magn. Reson*. **1989**, *84*, 204. (f) Hoffbauer, W.; Wefing, S.; Klösters, G.; Frick, F.; Jansen, M. *Solid State Nucl. Magn. Reson.* **1999**, *14*, 211.

(21) Karaghiosoff, K. In *Encyclopedia of Nuclear Magnetic Resonance*; Grant, D. M., Harris, R. K., Eds.; John Wiley: New York, 1996; Vol. 6, p 3612.

(22) Schindler, M.; Kutzelnigg, W. *J. Chem. Phys.* **1982**, *76*, 1919.

(23) Kutzelnigg, W.; Fleischer, U.; Schindler, M. *NMR* **1990**, *23*, 165.

(24) Bõhm, M. C.; Gleiter, R. *Z. Naturforsch*. **1980**, *36b*, 498.

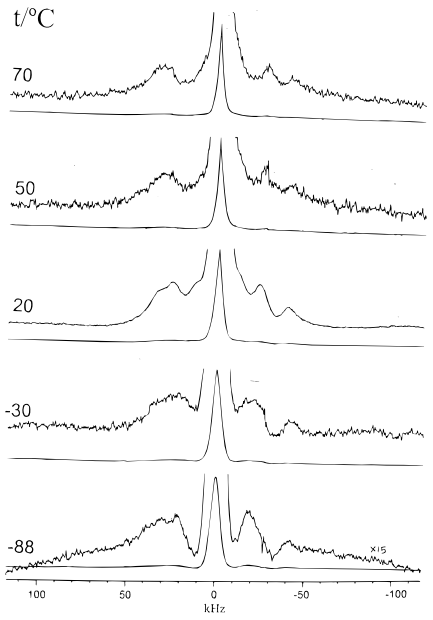

Figure 6. ^{7}Li NMR spectra of a nonspinning sample of Li_3P_7-(monoglyme)$_3$ as a function of the temperature as indicated. For each temperature, the upper trace was recorded at a 15-fold gain compared to the bottom one. The spectra were obtained by single pulse (2.1 μs) excitation with a recycle time of 30 s. The frequency scale is relative to an aqueous solution of $LiNO_3$.

the calculated orientations of the PAS's (see Figure 1c) for our dynamic line shape simulations. For the basal atoms the most shielded component, δ_{33}, is essentially parallel to the molecular C_3 axis, while the least shielded component, δ_{11}, lies in the symmetry plane containing the particular atom. The corresponding Euler angles (for their definitions see footnote to Table 1B) are therefore, 0, 0, γ, where γ is 0, 240° and 120° for atoms 1B, 2B, and 3B, respectively. For the equatorial atoms, δ_{11} is perpendicular to the symmetry plane, while δ_{33} lies within this plane and, depending on the model, is tilted by 61° or 52° to the C_3 axis. In our calculations we used an average value of 56°. The Euler angles for the equatorial atoms are accordingly 0, −56°, γ, where the γ's for 1E, 2E, and 3E are as above for the corresponding B atoms. Dynamic line shapes calculated with β(equatorial) = −61° or −52° were essentially indistinguishable from those calculated with $\beta = -56°$. For the apical atom the PAS is determined by symmetry. The calculated values of the CS anisotropy for this atom, $\Delta\delta = \delta_{11} - \delta_{33}$, are significantly smaller than the experimental one. But then, one has to keep in mind that the smaller anisotropies are more sensitive to the assumptions made in the calculations and the experimental analysis is more susceptible to errors in the measurements of the sideband intensities.

Simulation of the Dynamic Spectra. To simulate the dynamic spectra (Figures 3 and 4) we need to assume a suitable dynamic model. Two processes come to mind for solid Li_3P_7; 3-fold jumps about the C_3 symmetry axis of the P_7-cage, and bond shift rearrangement (or both). Before discussing the effect of these processes on the ^{31}P NMR spectrum in some detail we need to check whether the Li ions remain static or participate in the dynamic processes that take place in the system. To that end we recorded the ^{7}Li NMR spectrum of the compound over the temperature range where dynamic effects were observed in the phosphorus spectrum. The results, for a nonspinning sample, are shown in Figure 6. The center peak, corresponding to the $^1/_2 \leftrightarrow -^1/_2$ transition, and, at a higher gain, also the $\pm^3/_2 \leftrightarrow \pm^1/_2$ satellites, are clearly observed. From the shape of the

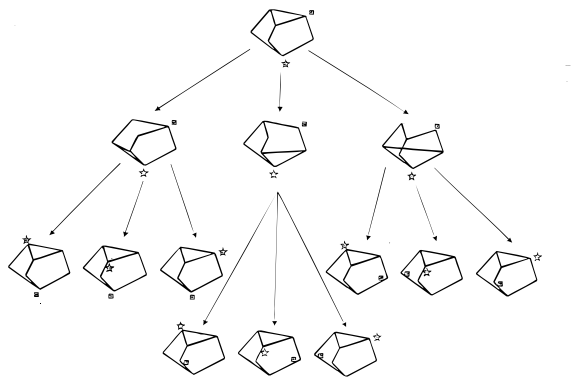

Figure 7. A schematic diagram representing the nine pathways of the combined bond shift rearrangement−reorientation in solid Li_3P_7. The first stage corresponds to the three possible bond shift channels for each P_7-cage. In the second stage the rearranged molecules rotate so as to end up in their original orientation in the lattice. Each molecule has three ways to do so, resulting in nine different permutations of the seven P-atoms in the P_7-cage. This is evident by comparing the final positions of P-atoms originally marked by a square (□) and by an asterisk (*).

spectra it appears that there are more than one type of lithium species in the sample. We have not attempted to sort them out. Although some minor changes may be observed in the structure of the satellites in the high temperature spectra compared to the low temperature ones, the main features of the spectra remain essentially unchanged upon increasing of the temperature. We take it to indicate that the Li ions do not take part in any dynamic process. In our kinetic analysis we shall therefore assume that only the P_7 anions are dynamic, while the lithium ions and ligand molecules remain immobile and form a rigid belt around the P_7-cages.

Referring to the high temperature traces in Figures 3 and 4, we note that the MAS spectrum consists of a single sideband manifold, while that of the nonspinning sample appears as a single, axially symmetric powder pattern. Such spectra can only result from a chemical process that interchanges all atoms in the P_7-cage. It must therefore involve the bond shift rearrangement (Figure 2a), with or without an independent 3-fold jumps process. In principle several mechanisms can be visualized for the rearrangement reaction in the solid state. In particular it could proceed without preserving the orientation of the P_7-cage, as in solution and perhaps in certain amorphous solids. However, for reasons outlined below we believe that in our Li_3P_7 compound the reaction proceeds, while retaining the orientation of the P_7-cage. One can imagine several kinetic pathways that will lead to this situation. We shall assume a model, similar to that shown to occur for the Cope rearrangement in bullvalene and many of its derivatives.[11−15] According to this model the rearrangement proceeds in concert with an overall reorientation of the P_7-cage, in such a way that it ends up in exactly the same orientation as it had originally. There are nine pathways for this to occur, as shown schematically in Figure 7. The first stage shows the three different chemical channels, ending in a rearranged, but "inverted" P_7-cage. Each of these intermediate states can then "physically" reorient in three different ways so as to end up in the same orientation as the molecule had originally. As may be seen in the figure, each of the nine pathways ends up in a different permutation of the P-atoms and therefore must be associated with a different exchange matrix. In setting up the overall exchange matrix we shall assume that all pathways are equally probable.

Support for this orientation-preserving mechanism (not necessarily with equal rates for all pathways) comes from the following consideration. The isotropic CS of the high-temperature average spectrum (−122 ppm) is very close to that calculated by averaging the low-temperature isotropic CS's of the seven atoms in the P_7-cage (−128 ppm). This is as expected for any rearrangement involving all the atoms in P_7. The small difference between the calculated and experimental values can be attributed to a temperature effect on the CS. However, we also find that the CS anisotropy, $\Delta\delta = \delta_{\parallel} - \delta_{\perp}$, of the average high-temperature spectrum (∼−250 ppm) is very close to that calculated by averaging the full CS tensors (expressed in the MF) over all the phosphorus atoms in the P_7-cage (−232 ppm). If the orientation were not preserved during the rearrangement, further averaging of the CS anisotropy would occur, resulting in a significantly reduced $\Delta\delta$. (Actually the same $\Delta\delta$ value would also be obtained if the P_7-cage would end up in an inverted orientation).

Assuming that all nine pathways in Figure 7 have equal probabilities leads to the following exchange matrix:

$$K_c = k_c \times \frac{1}{9}\begin{pmatrix} -9 & 0 & 0 & 2 & 2 & 2 & 3 \\ 0 & -9 & 0 & 2 & 2 & 2 & 3 \\ 0 & 0 & -9 & 2 & 2 & 2 & 3 \\ 2 & 2 & 2 & -8 & 1 & 1 & 0 \\ 2 & 2 & 2 & 1 & -8 & 1 & 0 \\ 2 & 2 & 2 & 1 & 1 & -8 & 0 \\ 3 & 3 & 3 & 0 & 0 & 0 & -9 \end{pmatrix}$$

where k_c is the rate constant for the reaction. In this matrix, the labeling of the rows and columns is in the order, 1B, 2B, 3B, 1E, 2E, 3E, and A. For the simulation of the dynamic MAS spectra we employed the formalism developed by Schmidt and Vega[25] using the framework of the Floquet theory, as described in detail for the case of bullvalene in ref 12. For the calculations we used the CS parameters of Table 1 and other parameters which are given in the caption of Figure 3. Examples of simulated spectra, so obtained, are shown on the right-hand side of that figure. On the right-hand side of Figure 4 are shown the corresponding simulated dynamic powder spectra for the nonspinning sample. These spectra were calculated by solving, for given orientations of the magnetic field in the MF (θ, φ), the corresponding Bloch−McConnell equations and summing the resulting line shapes over 3722 θ and φ values, using Conroy's algorithm.[26] In these equations the same kinetic matrix as described above was used and the NMR transitions frequencies were calculated from the expression

$$\omega^i(\theta,\varphi) = \omega_0[\delta^i_{zz}\, 1/_2(3\cos^2\theta - 1) + {}^1/_2(\delta^i_{xx} - \delta^i_{yy})\sin^2\theta\cos 2\varphi + \delta^i_{xy}\sin^2\theta\sin 2\varphi + (\delta^i_{xz}\cos\varphi + \delta^i_{yz}\sin\varphi)\sin 2\theta$$

where x, y, z are the coordinate axes in the MF, as defined in the footnote of Table 1B. The CS tensors in this frame were obtained from the corresponding ones in their respective PAS's (Table 1A) using the Euler angles given in Table 1B.

The simulated spectra displayed in Figures 3 and 4, were chosen so as to closely resemble the corresponding experimental traces. Since the MAS spectra appear to be more sensitive to dynamic effects and the neglect of dipolar interactions is better justified in their simulation, we concentrate our discussion on the former. These simulated spectra reproduce well the main features of the experimental results, in particular the initial broadening and the high-temperature coalescence into a single sideband manifold. However, in details the fit in the intermediate dynamic regime is far from perfect. We were unable to improve the fit by modifying the exchange matrix, for example, by including 3-fold jumps, by assigning different rate constant for the different pathways, or even by assuming a completely different mechanism for the bond shift rearrangement (see below). The disagreement between the experimental and various sets of simulated spectra may partly be of experimental origin; the spectra span a very wide frequency range (∼120 kHz), and they are not easily phased or subjected to baseline correction. Also, temperature gradients over the sample may cause lineshape distortions. Also, for the exchanged broadened spectra the signal-to-noise ratio is quite poor, and there may be additional impurity peaks that may become conspicuous in this regime. We feel, however, that the disagreement also reflects real effects.

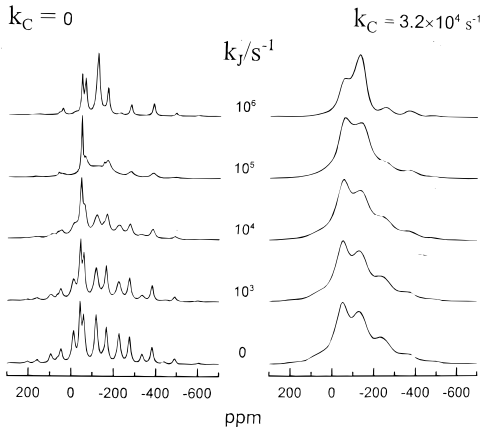

Figure 8. Simulated ^{31}P dynamic MAS spectra of the P_7-cage in the presence of 3-fold jumps. In the left column it is assumed that no concomitant Cope rearrangement takes place. The spectra on the right were calculated on the assumption that a Cope rearrangement at a rate of $3.2 \times 10^4\ s^{-1}$ takes place in concert with 3-fold jumps at the indicated rates. The calculations were done as described in the caption of Figure 3.

First, since our sample is amorphous, we cannot rule out a heterogeneous situation, with a spatial distribution of mechanisms and rate constants. Even for a homogeneous situation the local symmetry around the P_7-cage is not perfectly C_{3v}. The probability of the nine pathways may therefore not be exactly the same, as assumed in the simulations. We have, in fact, simulated spectra with different weights for the different pathways and observed corresponding effects on the line shapes. However, the number of alternatives is so vast that it is quite hopeless to obtain a unique model by scanning all the alternatives. We also considered a mechanism in which the first bond shift is concertedly followed by a second rearrangement of one of the newly formed bonds between the basal atoms. This process requires only a small physical reorientation of the P_7-cage. However, the resulting line shapes did also not improve the fit with the experimental results. Finally we considered the effect of 3-fold jumps on the spectrum. As discussed above, this process alone cannot account for the observed changes in the spectra. Since this process preserves the identity of the three types of P-atoms in the P_7-cage, it will end up (in the fast-exchange regime) in an average spectrum consisting of three sideband manifolds, contrary to observation. A sequence of dynamic MAS spectra calculated for this model is shown on the left-hand side of Figure 8. The exchange matrix used for

(25) Schmidt, A.; Vega, S. *J. Chem. Phys.* **1987**, *87*, 6895.
(26) Conroy. H. *J. Chem. Phys.* **1967**, *47*, 5307.

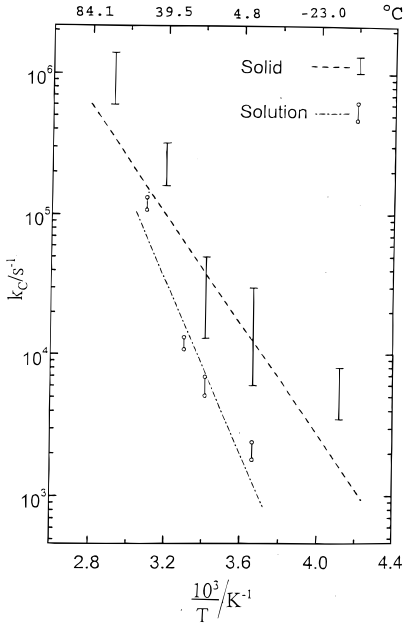

Figure 9. A plot of the estimated rate constants for the bond shift rearrangement in solid $Li_3P_7(monoglyme)_3$ (from the present work) and in a THF solution (calculated from spectra published in ref 5) as a function of the inverse absolute temperature. The bars indicate the range of "acceptable" fit between the simulated and experimental spectra. The dashed lines serve to aid to distinguish between the solid state and solution results.

these simulations is shown below, where the labeling of the rows and columns is as for the rearrangement matrix and k_J is the rate constant for the 3-fold jumps process.

$$K_J = k_J \times \frac{1}{2}\begin{pmatrix} -2 & 1 & 1 & 0 & 0 & 0 & 0 \\ 1 & -2 & 1 & 0 & 0 & 0 & 0 \\ 1 & 1 & -2 & 0 & 0 & 0 & 0 \\ 0 & 0 & 0 & -2 & 1 & 1 & 0 \\ 0 & 0 & 0 & 1 & -2 & 1 & 0 \\ 0 & 0 & 0 & 1 & 1 & -2 & 0 \\ 0 & 0 & 0 & 0 & 0 & 0 & 0 \end{pmatrix}$$

We cannot, however, rule out the possibility that 3-fold jumps occur simultaneously and independently of the bond shift process. We therefore attempted to match the experimental spectra with a model, in which both processes occur simultaneously, by setting up an exchange matrix of the form

$$K = k_J K_J + k_C K_C$$

One set of such simulated spectra is shown on the right-hand side of Figure 8. In this simulation k_C was fixed at 3.2×10^4 s^{-1} and k_J was varied as indicated in the figure. There are clear effects on the calculated line shapes, but again, the number of combinations is huge, and the spectrum quality is insufficient to ascertain or to rule out a concomitant jump process.

We thus end up with only one confirmed dynamic process, that is, that of the bond shift rearrangement. Assuming it to be the only one responsible for the ^{31}P NMR line broadening in solid Li_3P_7, an estimate of its rates as a function of the temperature was obtained by "eye fitting" the experimental spectra with a series of simulated ones. While this method is certainly not satisfactory for accurate determination of the rates, it does provide for each spectrum a range of "acceptable" rates. These ranges are plotted as bars in Figure 9. From these results activation energy ranging between 7 and 12 kcal/mol can be estimated, with k_C at room temperature of about 10^5 s^{-1}. In Figure 9 are also plotted rate constants for the bond shift rearrangement in a THF solution, which we computed from spectra published by Baudler et al.[5] using the exchange matrix

$$K^{THF} = k_C^{THF} \times \frac{1}{3}\begin{pmatrix} -3 & 2 & 3 \\ 2 & -2 & 0 \\ 1 & 0 & -3 \end{pmatrix}$$

where the rows and columns are labeled in the order, B, E, and A. The estimated activation energy in this solvent (11−15 kcal/mol) overlaps the estimated range for the solid sample. (The calculated[24] activation energy for the free P_7 trianion is 14.1 kcal/mol). However, the actual rate at room temperature is definitely higher in the solid, by more than a factor of 5, than it is in solution. In fact, the effect is even bigger, if we recall that the rate of each bond shift channel in the solid actually corresponds to $3k_C$.

Summary and Conclusions

We have investigated the ^{31}P NMR spectrum of a solid sample of $Li_3P_7(monoglyme)_3$ in the temperature range −90−70 °C. In the range −30−70 °C the spectra exhibit conspicuous dynamic effects that were interpreted in terms of the bond shift rearrangement of the P_7-cage, in analogy with the well-known Cope rearrangement in bullvalene. Although our sample was amorphous, it appears that the process proceeds while retaining the orientation of the P_7-cage. The solvated Li ions seem to form a rigid framework, which holds the P_7-cages inside fixed pores. During the rearrangement process the P_7-cages pass through an intermediate "soft" stage, which allows them to reorient and acquire their original orientation in the pores. It is interesting to note that the rate of this process is faster in the solid state than it is in solution[5] (10^5 as compared with 1.5×10^4 s^{-1} at room temperature). Perhaps, the rigid lattice of the solvated Li network provides large enough pores that facilitate the rearrangement, while at the same time the electrostatic potential provided by the Li^+ belt forces the P_7-cages to retain their orientations. In solution, on the other hand, there is apparently strong interaction between the P_7 anion and the solvent molecules, resulting in a higher hindrance for the rearrangement process. In the analogous case of bullvalene the kinetic parameters for the Cope rearrangement in the solid and in solution were found to be essentially the same. This may be rationalized by the fact that bullvalene is a neutral molecule and therefore less affected by electrostatic interactions.

Although there seems to be no doubt about the identification of the bond shift rearrangement as the major cause for the line broadening effects in the ^{31}P NMR spectra of solid Li_3P_7, we were unable to fit them quantitatively to simulated dynamic line shapes. This is partly due to experimental artifacts and perhaps partly also to the neglect of the dipolar interaction in the simulations. However, the discrepancy may also reflect real effects. For example due to the lack of C_3 symmetry at the site of the P_7-cage, the different pathways of the reaction (Figure 7) may have different rates. This was, in fact, found to be the case in solid bullvalene.[13] Also, due to the amorphous nature of our sample, there may be a spatial distribution of rate constants and pathways for the rearrangement reaction, which would undermine our attempts to quantitatively analyze the dynamic line shapes. It would therefore be advantageous to extend the study to solvated Li_3P_7 compounds that can be obtained in a crystalline form, for example $Li_3P_7(tmeda)_3$.[2]

Acknowledgment. This work was supported by the G.I.F (German-Israeli Foundation) Grant No. I558-218.05/97, by the

G.M.J. Schmidt Minerva Center for Supramolecular Architecture and by the U.S. National Science Foundation under Grant No. CHE-9707202. We thank Elena Vinogradov for providing the program used to simulate the powder line shapes with the dipolar interaction included.

JA992452L